AIAA-94-0603

A Numerical Study of the Spray Characteristics of the UIUC Subsonic Wind Tunnel

A. Khodadoust
M.B. Bragg

University of Illinois at Urbana-Champaign

32nd Aerospace Sciences Meeting & Exhibit
January 10-13, 1994 / Reno, NV

A NUMERICAL STUDY OF THE SPRAY CHARACTERISTICS OF THE UIUC SUBSONIC WIND TUNNEL

Abdollah Khodadoust[+] and Michael B. Bragg[*]
University of Illinois at Urbana-Champaign

ABSTRACT

The behavior of water droplet trajectories in the two-dimensional subsonic wind tunnel at the University of Illinois was studied numerically. A finite-difference two-dimensional potential flow solver and a three-dimensional particle trajectory code have been written and validated for solving the flowfield inside of a subsonic incompressible flow wind tunnel and computing particle trajectories. Seven droplet sizes ranging from 6.31 to 45.19 microns were used in this study based on the Langmuir-D distribution for a mean volumetric diameter of 20.36 microns. The droplets were released upstream of the contraction in the inlet of the wind tunnel. The results of this computational study showed that the trajectory of the larger water droplets were affected by the droplet inertia and gravity more dramatically than that for the smaller particles. The calculated liquid water contents at a perpendicular plane in the center of the test section indicated a high concentration of large droplets near the tunnel centerline, whereareas the smaller droplets can be expected to span the entire test section width. The analysis further revealed that the computed effective droplet distribution was skewed toward the larger droplets in comparison with the Langmuir-D distribution.

NOMENCLATURE

symbol	description
C_D	droplet drag coefficient
CR	tunnel contraction ratio
Fr	Froude number
g	gravitational acceleration constant
H	tunnel height
K	droplet inertia parameter
K_0	modified inertial parameter
LWC	liquid water content
MVD	mean volumetric diameter
N	dummy-dependent variable for Poisson system inversion
R_U	droplet Reynolds number
S	stream function
t	time
U	tunnel velocity
u	local velocity in x-direction
v	local velocity in y-direction
x	global x-coordinate
y	global y-coordinate
Y_i	tunnel inlet height
δ	droplet diameter
η	droplet non-dimensional position
ρ	air density
σ	droplet density
τ	non-dimensional time$=\frac{Ut}{Y_i}$
$(\bar{\ })$	vector quantity
$(\dot{\ })$	first derivative with respect to τ
$(\ddot{\ })$	second derivative with respect to τ

INTRODUCTION

During flight in adverse weather conditions, an aircraft's flight components are subjected to water droplet impingement. Given the proper conditions, the impinging water may freeze on the flight surface and render that component partially or totally ineffective. De-icing is one of the techniques that is currently used to battle the problem. In order to determine the extent of the flight surface which is to be protected by the de-icing equipment, it is necessary to develop a technique which predicts the impingement limits on that flight component.

Computational methods have been developed to determine impingement limits and impingement efficiency on airfoils and wings[1-5]. Wind tunnel tests have been conducted in icing tunnels to measure impingement characteristics for code validation[6-8]. While the existing codes calculate the impingement efficiency in free air, the validation studies are performed in wind tunnels where the tunnel walls can affect the droplet trajectories. The wall effects have been found to be small and within the limits of experimental error for most two-dimensional airfoil testing for a typical subsonic tunnel test section without accounting for the upstream inlet contraction effects on the water droplets[9]. Effects of the wind tunnel walls on the computed trajectories in a three-dimensional flowfield with a reflection-plane mounted

[+] Postdoctoral Research Associate, Department of Aeronautical & Astronautical Engineering, University of Illinois at Urbana-Champaign, Member AIAA.

[*] Associate Professor, Department of Aeronautical & Astronautical Engineering, University of Illinois at Urbana-Champaign, Associate Fellow AIAA .

rectangular wing are currently under investigation[10].

The present technique includes the contraction effects upstream of the test section. This study is a part of the initial phase of a multi-phase program whose ultimate goal is to provide data for code validation. A computer code has recently been developed[11] which provides the capability to predict impingement characteristics for three-dimensional rotating bodies.

Since the validation experiments are to take place inside of a wind tunnel, it is desirable to know the effect of the tunnel walls on the cloud distribution in the test section. The spray is assumed to be generated upstream of the tunnel contraction through a pressurized spray rig system. This study will be beneficial in determining appropriate spray nozzle locations, which would provide a uniform cloud distribution in the test section. The results of the computation can also be used in correcting the LWC and droplet size distribution effects due to the tunnel walls.

NUMERICAL FORMULATION

Flowfield

The flowfield solution technique employed here was used by Coirier[12,13] to study the effect of screens on two-dimensional inlets using a finite-difference method for subsonic inviscid incompressible flow. The stream function S satisfying the continuity equation is defined such that the velocity field is given by

$$u = \frac{\partial S}{\partial y} \tag{1}$$

$$v = -\frac{\partial S}{\partial x} \tag{2}$$

Substitution in the X and Y momentum equations leads to the following Poisson equation:

$$S_{XX} + S_{yy} = \frac{\partial H_S}{\partial S} \tag{3}$$

where $\partial H/\partial S$ is defined as the source term P(S). Introducing a Laplace equation of a different variable N as

$$N_{xx} + N_{yy} = 0 \tag{4}$$

and inverting the Poisson system yields the following elliptic partial differential equations which are solved in the rectangular computational domain:

$$AX_{ss} - 2BX_{sn} + CX_{nn} = -J^2(PX_s) \tag{5}$$

$$AY_{ss} - 2BY_{sn} + CY_{nn} = -J^2(PY_s) \tag{6}$$

$$A = X_n^2 + Y_n^2 \tag{7}$$

$$B = X_s X_n + Y_s Y_n \tag{8}$$

$$C = X_s^2 + Y_s^2 \tag{9}$$

$$J = X_s Y_n - X_n Y_s \tag{10}$$

These equations determine the X and Y locations of the constant S (streamlines) and constant N on the physical domain. The transformation yields the flow streamlines, thus the generation of the grid directly yields the velocity field. Figure 1 shows the computational grid in the physical domain with the inflow and outflow planes set one inlet length upstream and downstream of the inlet and exit planes respectively. This boundary placement will allow the flow angle distribution to smoothly approach zero at the inflow and outflow planes.

Equations 5 and 6 were solved using second-order central and one-sided finite differences in a successive line-relaxation method. The value of the stream function S on the upper and lower boundaries and the flow angle at the inflow and outflow planes served as the boundary conditions on the rectangular computational domain. The value of head loss or P(S) was set to zero for this study.

Particle Trajectory

Assuming a low concentration of spherical droplets of constant mass, Newton's second law of motion in non-dimensional form yields[14,15]

$$\ddot{\bar{\eta}} = \frac{1}{K}\left(\frac{C_D R}{24}\right)\left(\frac{\bar{u}}{U} - \dot{\bar{\eta}}\right) + \frac{1}{Fr^2}\frac{\bar{g}}{g} \tag{11}$$

where the droplet inertia parameter is given by

$$K = \frac{\sigma \delta^2 U}{18 Y_i \mu} \tag{12}$$

and the Froude number, Fr is given by

$$Fr = \frac{U}{\sqrt{Y_i g}} \tag{13}$$

and the droplet Reynolds number R_U is given by

$$R_U = \frac{\rho U \delta}{\mu} \tag{14}$$

and

$$R = R_U \left| \frac{\bar{u}}{U} - \frac{\dot{}}{\eta} \right| \qquad (15)$$

The velocity $\bar{u}/U$ in Eqs. 11 and 15 above are determined by interpolation of velocities obtained from the finite-difference solution of the flowfield.

The particle drag is calculated by the method of Langmuir and Blodgett[16] which yields the following form in the trajectory equation above:

$$\frac{C_D R}{24} = 1.0 + 0.197R^{0.63} + 2.6x10^{-4} R^{1.38} \qquad (16)$$

Given the droplet initial conditions in addition to the free stream and droplet size data, the trajectory equation is numerically solved by a predictor-corrector scheme due to Gear[17].

Through the principle of mass conservation in a droplet stream tube,

$$LWC_1 \, U_1 \, A_1 = LWC_2 \, U_2 \, A_2 \qquad (17)$$

or

$$LWC_2 = LWC_1 \frac{U_1}{U_2} \frac{A_1}{A_2} \qquad (18)$$

where the subscripts (1) and (2) denote conditions upstream of the contraction and in the test section, respectively. The area ratio A_1/A_2 is determined from the trajectory calculations. If the droplet velocities are assumed to equal to the tunnel velocity at locations (1) and (2), then the velocity ratio U_1/U_2 is the tunnel contraction ratio. The LWC in the test section, LWC_2, is calculated using Eq. 18 with respect LWC_1 at the droplet release plane, which is assumed to be unity.

CODE VALIDATION

The validation of the code was carried out in two steps. First, the flowfield calculations were validated, and in the second step, trajectory computations were authenticated. The flowfield was validated by comparing the computer solution to the analytical solution for a known inlet geometry. For an arbitrary two-dimensional contraction with constant vorticity everywhere in the flowfield, the analytical solution for the u-velocity profile may be obtained at the inflow plane by[12]

$$u_1 = -\omega Y_1 + \frac{\omega Y_i}{2} + \frac{1}{CR} \qquad (19)$$

and at the outflow plane by

$$u_2 = -\omega Y_2 + \frac{\omega Y_i}{2CR} + 1 \qquad (20)$$

The subscripts (1) and (2) denote conditions at the inflow and the outflow planes respectively, Y_i denotes the inlet height, and CR is the tunnel contraction ratio. The v-velocity is set to zero by imposing the Neumann boundary condition at the inflow and outflow planes. Figures 2 and 3 show the comparison of the inflow and outflow u-velocity profiles for two values of vorticity ω = -.1 and -.3 . Examination of the profiles shows that the computed and predicted profiles compare quite well. The computed and the predicted profiles agreed to within 3 decimal places. Figure 4 shows the resulting streamlines for ω=-.3 case. Here the correspondence between the linear inflow u-velocity profile and the streamline distribution is clearly shown. By definition of the stream function, mass must be conserved between the streamlines. Near the tunnel wall at the inflow plane the streamlines are closely spaced due to increased velocity. On the lower portion of the inflow plane, the streamlines are placed further apart due to lower velocity in this region of the inflow plane velocity profile.

The trajectory computations are validated by comparing the computed trajectories by the present method to those computed by Wells[9] in a rectangular duct with no contraction effects. Figure 5 shows the comparison of the calculated trajectories for a 20.36 micron water droplet at a tunnel velocity of 100 mph. The water droplet was released at the beginning of the duct with the same streamwise velocity as the flow. An additional cross-flow velocity of 40 mph was imposed on the droplet in order to compare the trajectories both in the x- and y-directions. In the method used by Wells and Bragg, the droplet inertia term, in addition to the Froude number and the non-dimensional time τ are made non-dimensional using the chord length of an airfoil mounted in the test section. Since no airfoil is included in the present analysis, the length scale for the empty test section is chosen to be the tunnel inlet height. Both methods of computation show the 20.36 micron droplet looses the cross-flow velocity component rapidly and maintains only a streamwise flow component after 0.01 seconds after injection in the tunnel. The computed trajectories using the different length and time scales appear to agree quite well, thus providing confidence in the trajectory computations using the present method. Note that the inset graph in Fig. 5 shows the computed trajectory of Wells deviates from the trajectory computed by the present method as x/Y_i =2.0 is approached. Since the vortex panel method of Wells

places an airfoil in the test section, the computed incoming trajectories in that code anticipate the presence of the airfoil by adjusting to the flowfield of that airfoil.

RESULTS AND DISCUSSION

The flowfield solution is shown in Fig. 6. The computational domain, along with velocity and pressure coefficient profiles are shown in this figure. The u-component of velocity is seen to start at 1/6th the final value in the test section. This is consistent with the conservation of mass principle whereby the increased velocity in the test section is proportional to the area ratio in subsonic incompressible flow. The v-component of the velocity conforms to the Neumann boundary condition of no cross-flow velocity placed at the inflow and outflow planes. Near the contraction region of the tunnel, it takes on negative values with a maximum at x/Y_i =1.5 and then recovers to zero rapidly downstream of the contraction. The pressure coefficient is calculated from the classical relation

$$C_p = 1 - \frac{u^2 + v^2}{U^2}. \qquad (21)$$

The pressure coefficient is at it's highest value of nearly one at the beginning of the inflow plane. As the test section is approached the velocity increases and causes a drop in the pressure coefficient to a value of zero downstream of the contraction at x/Y_i = 2.

This study is intended to provide clues to the droplet behavior and distribution in the test section of the UIUC subsonic wind tunnel. The tunnel contraction takes place in the xy-plane, with gravity acting in the (-z)-direction, which is into the page in Fig. 1. The tunnel has a contraction ratio of six and a test section height and length of 10 and 60 inches, respectively. The characteristics of the spray nozzles which are mounted in the tunnel were used to determine a suitable range of droplet sizes for this analysis. Operating at a pressure ratio of 0.65, the nozzles produce droplets with a MVD of 20.36 micron[7]. Assuming a Langmuir-D distribution, Fig. 7[7], seven droplet sizes ranging from 6.31 to 45.19 microns were considered.

Figure 8 shows the computed trajectories for the 10.58 micron droplets. The trajectories were initiated at the same x-location, varying in y-location across the tunnel span. The droplets appear to follow the flow closely when released across all y-locations. This is in contrast with the trajectories shown in Fig. 9 for the 45.19 micron drop size. Due to the larger droplet size and mass, the released droplets do not negotiate the turn in the tunnel contraction region. The droplets' inertia carry them near the tunnel centerline downstream of the contraction. This difference in behavior is further illustrated in Fig. 10 where the computed trajectories for both droplet sizes are compared at two different y-locations. At both release locations y/Y_i = 0.1 and 0.3, the larger droplet overshoots the smaller droplet and approaches closer to the tunnel wall before overshooting again due to the contraction at the beginning of the test section. The larger droplets carry more mass and therefore inertia, and as a result, their ability to conform to the flowfield in regions of high flow gradient is reduced in comparison with smaller droplets.

Since the droplets have size and mass, it is anticipated that their motion will be affected by gravity in addition to the flowfield itself. Droplet fallout for the 10.58 micron droplet is shown in Fig. 11. The droplet is released at the same x-z plane at different y-locations. The droplet released at y/Y_i =0.49 has the furthest distance to travel before reaching the test section while the droplet released at y/Y_i =0.05 has the shortest travel distance. Consequently, the fallout for the furthest location from the test section is the largest and vice versa. The fallout rate is the slope of the droplet fallout trajectory. Note that due to variation of the tunnel flowfield across the tunnel prior to test section, the fallout rates are different for the droplets released at different y-locations. Once past the tunnel contraction where flow uniformity has been achieved, the fallout rates appear to be same.

The same conditions are shown for the 45.19 micron droplet in Fig. 12. The overall behavior here is the same as that for the smaller droplet shown in Fig. 11. Due to the larger droplet size, the maximum fallout is computed to be 0.18 inches over a distance of 8 feet. The maximum fallout for the smaller droplet is computed to be 0.018 inches over a distance of 8 feet. This difference in the fallout and their rates is illustrated in Fig. 13 where the computed fallout trajectories for the 10.58 and 45.19 micron droplets are compared for two y-locations across the tunnel. The main parameter affecting the fallout is the Froude number of the flow which is independent of the droplet size and mass. Froude number appears in the second term on the right-hand side of the droplet motion equation. In the absence of other body forces, it acts only in the direction of gravity.

In order to investigate the mass distribution across the test section, the liquid water content (LWC) in the test section must be estimated. The trajectories for seven droplet sizes based on the Langmuir-D distribution were computed across the tunnel from x/Y_i =0.8, which is the location of the spray nozzles, to x/Y_i=2.5 which is the center of the test section.

The computed LWC's in the test section for

the seven droplet sizes are shown in Fig. 14. The distributions shown are not weighted by the Langmuir-D distribution. They show the LWC for each droplet size as if a separate monodisperse cloud was tested at each droplet size. The plot shows that while the smaller droplets can be expected to cover the entire width of the test section, a large concentration of heavier particles should be expected near the tunnel centerline.

Now consider an initial cloud at the nozzle plane which has a Langmuir-D distribution with LWC=1. If the tunnel walls had no effect on the droplet trajectories, a Langmuir-D distribution with LWC=1 would be expected at the test section. However, due to the tunnel wall effects in the inlet, LWC and the droplet size distribution will vary across the test section span.

Figure 15 shows the concentration of mass of water as a function of droplet size for various stations across the tunnel test section. The area under each curve is proportional to the amount of water, i.e. the LWC, which is present in the airstream at each spanwise location y/Y_i. The Langmuir-D distribution is shown for reference in this figure. Due to the tunnel effects, the concentration curves at different y/Y_i's do not match with the Langmuir-D distribution. The effect of the tunnel walls is further illustrated in Fig. 16 where the total LWC is plotted for various locations in the test section.

In an experimental study, the test section LWC is measured using a reference collector. Therefore, the effect of the tunnel walls on the LWC can effectively be corrected for when reducing impingement data. However, the effect of the tunnel walls on the droplet size distribution is not so easily measured or corrected.

When each curve is made non-dimensional with respect to it's area, which is proportional to the total LWC for that location in the test section, the variation in the drop size distribution as a function of test section location becomes more apparent. This is shown in Fig. 17 for various test section locations. Since the droplet size distribution varies from that which yields a MVD of 20.36 microns based on the Langmuir-D distribution, it would be logical to calculate new MVD's based on the new distributions. In order to determine the new MVD's for each y-station across the test section, the cumulative fraction of total LWC for each y-station is added up in cumulative fashion as a function of droplet size. These values are plotted and shown in Fig. 18 for various test section locations. The MVD droplet size is one which carries 50 percent of the cumulative fraction of the total LWC. The effective MVD's across the test section are shown in Fig. 19. For locations near the tunnel centerline ($y/Y_i < 0.035$), the MVD is larger than 20.36 microns. Outside of this range, only the smaller droplets are present and therefore the effective MVD is lower than 20.36 microns. This expected re-distribution or sorting of the particles is due to the effects of the tunnel contraction.

CONCLUSION

The results from a flowfield solver and a particle trajectory solver were presented. The flowfield and trajectory solutions matched well with other established techniques. The method was used to compute the flowfield and droplet trajectories inside of a subsonic incompressible wind tunnel. The tunnel and droplets were modeled after those which are in use for impingement validation studies for BFGoodrich Aerospace.

Results were presented for a Langmuir-D distribution with a 20.36 micron MVD droplet, resulting in seven droplet sizes ranging from 6.31 micron to 45.19 micron in diameter. The computed droplet fallout due to gravity was negligible for all droplet sizes, less than 0.2 inches over eight feet of travel.

The computed trajectories for the droplets showed that the lighter particles followed the flow more closely than the heavier droplets in regions of high flow gradient, as expected. The contraction region of the tunnel presents such a region where large velocity changes exist. The larger droplets are not able to negotiate the large velocity gradients immediately upstream of the test section and as a result, a large concentration of heavier droplets near the tunnel centerline is observed.

The calculated concentrations at the test section were presented for the seven droplet sizes in this analysis. Due to a high concentration of large droplets near the tunnel centerline in the test section, LWC values near the tunnel centerline were larger than those for a Langmuir-D distribution. This also indicates that the effective MVD of the distributions are skewed towards the larger droplets in the Langmuir-D distribution.

In terms of the experimental droplet impingement to be carried out in the test section, the larger LWC values can be ignored since they are accounted for by the measurement of a reference LWC value through the reference collector. The change, or sorting, of the droplet size distribution, which is due to the tunnel contraction effects, can not be ignored however. This means that due to the tunnel contraction effects, a uniform cloud distribution at the tunnel inlet will not result in a uniform distribution in the test section.

This analysis represents an exploratory study of the tunnel contraction effects on the droplet motion and distribution in a subsonic incompressible wind tunnel. Tunnel wall effects were found to have a significant effect on droplet distribution in the test

section. Results of this analysis can be extended to identify the proper initial cloud distribution in the tunnel inlet in order to obtain a final uniform distribution in the test section. Further analysis can be carried out by incorporating more detailed spray nozzle characteristics. This would include allowing for a non-uniform initial cloud distribution, turbulent mixing, and droplet evaporation as factors in the calculation of droplet distribution in the test section.

ACKNOWLEDGMENT

This work was supported in part by B.F.Goodrich De-Icing Systems, Uniontown, Ohio.

REFERENCES

1. Norment, H. J., "Calculation of Water Drop Trajectories to and About Arbitrary Three-Dimensional Bodies in Potential Airflow," NASA CR 3291, 1980.

2. Gent, R. W., Calculation of Water Droplet Trajectories About an Airfoil in Steady, Two-Dimensional, Compressible Flow," RAE TR 84060, June 1984.

3. Lozowski, E. P. and Oleskiw, M. M., "Computer Modeling of Time-Dependent Rime Icing in the Atmosphere," CRREL 83-2, Jan. 1983.

4. Kim, J. J., "Computational Particle Trajectory Analysis on a Three-Dimensional Engine Inlet," AIAA-85-0411, 23rd Aerospace Sciences Meeting, Reno, Nevada, Jan. 1985.

5. Ruff, G. A. and Berkowitz, B., "User's Manual for the NASA Lewis Ice Accretion Code (LEWICE)," NASA CR-185129, 1990.

6. Gelder, T. F., Smyers, W. H., and von Glahn, U., "Experimental Droplet Impingement on Several Two-Dimensional Airfoils with Thickness Ratios of 6 to 16 Percent," NACA TN 3839, 1956.

7. Papadakis, M., Elangonan, R. Freund, G. A. Jr., Breer, M., Zumwalt, G. W., and Whitmer, L. , "An Experimental Method for Measuring Water Droplet Impingement Efficiency on Two- and Three-Dimensional Bodies," NASA CR 4257, November 1989.

8. Tennison, G., Bragg, M. B., and Farag, K., "A Comparison of a Droplet Impingement Code to Icing Tunnel Results," AIAA-90-0670, 28th Aerospace Sciences Meeting, Reno, Nevada, Jan. 8-11, 1990.

9. Wells, S. L. and Bragg, M. B., "A Computational Method for Calculating Droplet Trajectories Including the Effects of Wind Tunnel Walls," AIAA 92-0642, 30th Aerospace Sciences Meeting, Reno, Nevada, Jan. 6-9, 1992.

10. Farag, K. and Bragg, M. B., "The Effects of Wind Tunnel Walls on Droplet Trajectories in the Vicinity of a 3D Wing," AIAA-94-0644, 32nd Aerospace Sciences Meeting, Reno, Nevada, Jan. 10-15, 1994.

11. Farag, K., Bragg, M. B., Martin, C., Daneshgar, G., "Three-Dimensional Droplet Trajectory Method for Propellers," AIAA-92-0644, 30th Aerospcae Sciences Meeting, Reno, Nevada, Jan. 6-9, 1992.

12. Coirier, W. J., "A Computational Method for the Analysis of Low Speed Wind Tunnel Inlets with Screens, Using an Application of Elliptic Grid Generation," Master's Thesis, The Ohio State University, Columbus, Ohio, March 1985.

13. Coirier, W. J. and Bragg, M. B., "Computational Method for Screened Two-Dimensional Wind Tunnel Inlets," Journal of Aircraft, vol. 24, no. 4, April 1987, pp. 281-283.

14. Bragg, M. B., "Rime Ice Accretion and its Effect on Airfoil Performance," PhD dissertation, Ohio State University, 1981, also NASA CR 165599.

15. Bragg, M. B., "A Similarity Analysis of the Droplet Trajectory Equation," AIAA Journal, vol. 20, no. 12, Dec. 1982, pp. 1681-1686.

16. Langmuir, I. and Blodgett K., "A Mathematical Investigation of Water Droplet Trajectories," AAFTR 5418, February 1946.

17. Gear, C. W., "DIFSUB for Solution of Ordinary Differential Equations," Comm. ACM 14, March 1971, pp. 785-790.

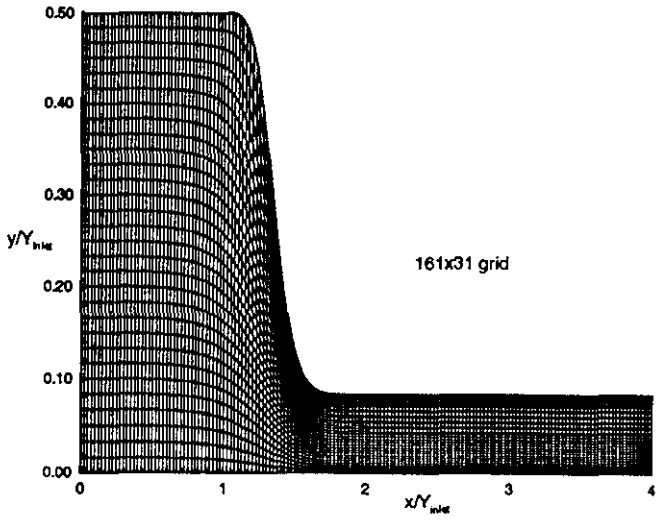

Fig. 1 Computational Grid in the Physical Domain.

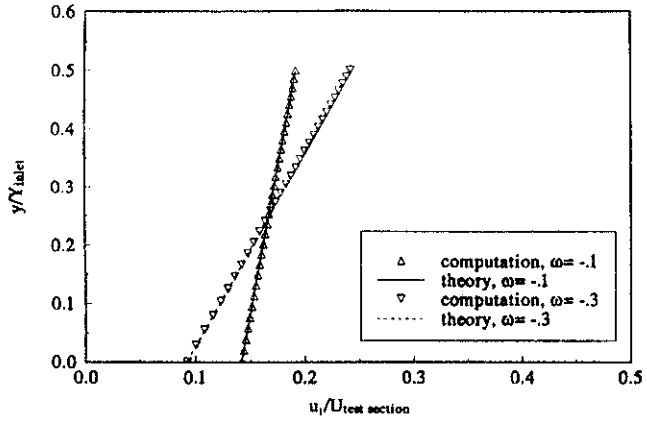

Fig. 2 Comparison of Inflow Velocity Profiles for ω = -0.1 and -0.3.

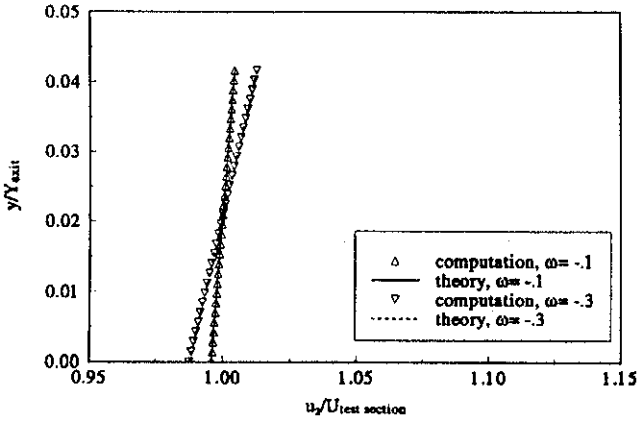

Fig. 3 Comparison of Outflow Velocity Profiles for ω = -0.1 and -0.3.

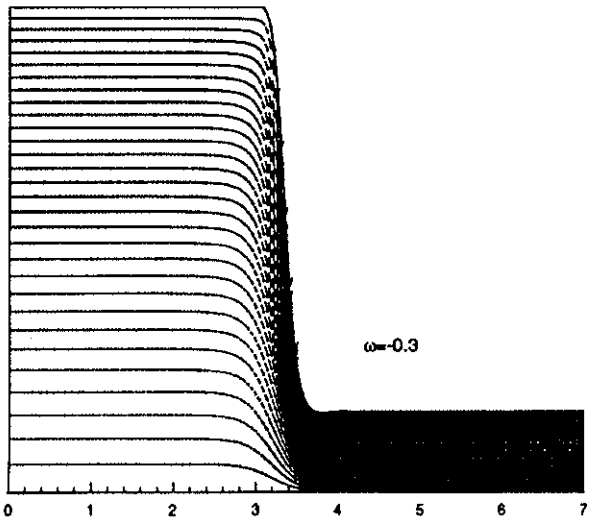

Fig. 4 Flowfield Streamlines for ω = -0.3.

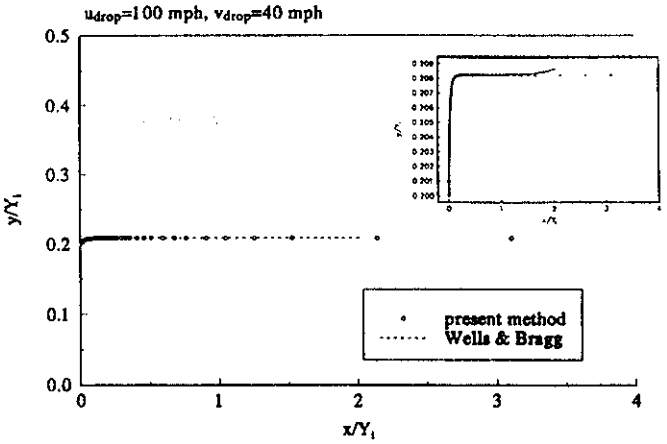

Fig. 5 Comparison of the Computed Trajectories.

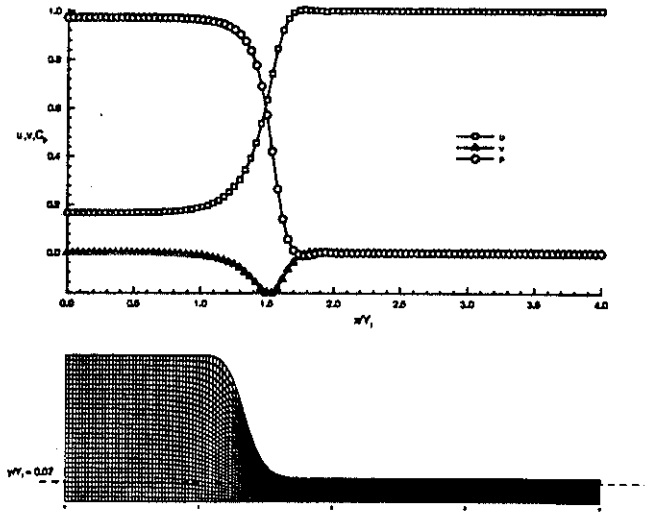

Fig. 6 Computed Flowfield Profiles for y/Y_i = 0.07.

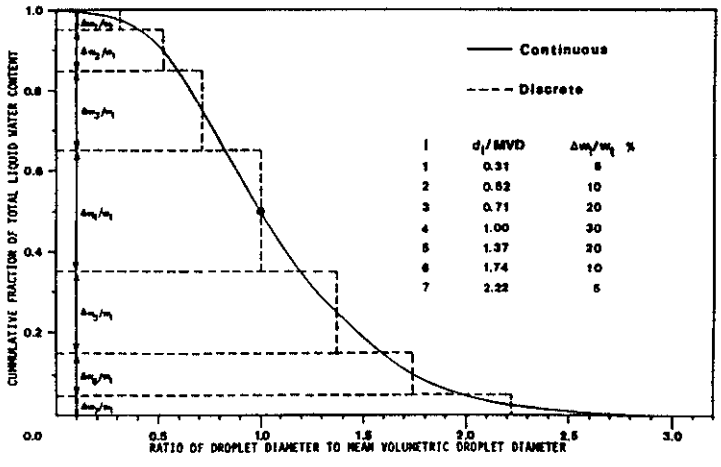

Fig. 7 Langmuir-D Dimensionless Distribution of Droplet Sizes Used for the Current Droplet Trajectory Analysis

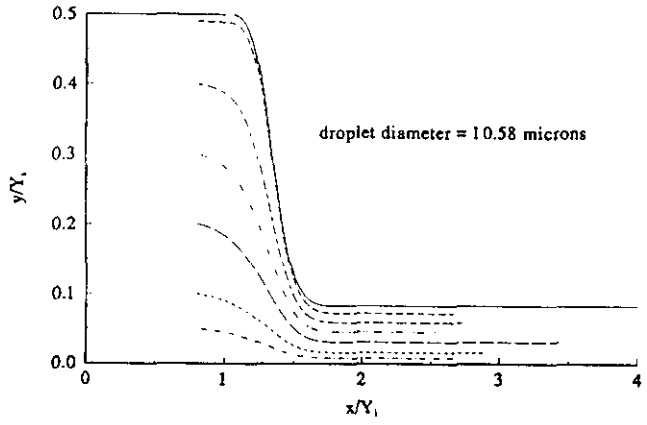

Fig. 8 Computed Droplet Trajectories for the 10.58 micron Droplet, U=175 mph.

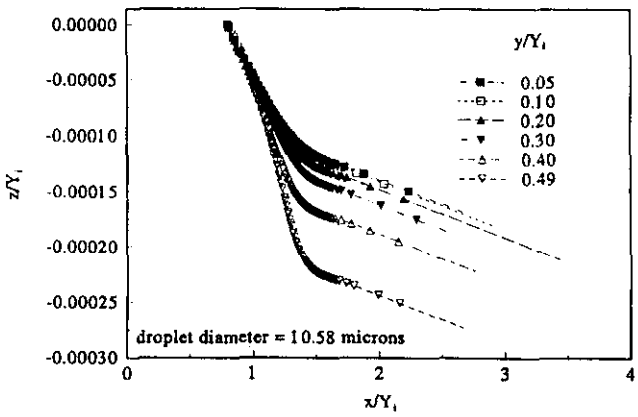

Fig. 11 Computed Droplet Fallout for the 10.58 micron Droplet, U=175 mph.

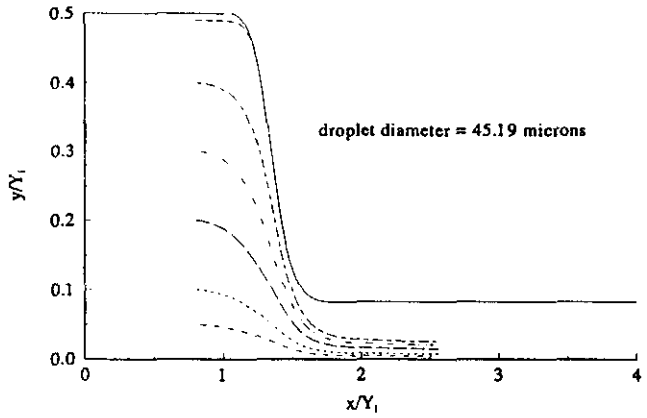

Fig. 9 Computed Droplet Trajectories for the 45.19 micron Droplet, U=175 mph.

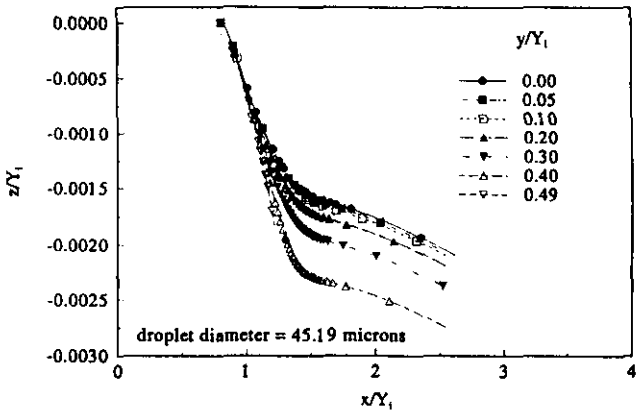

Fig. 12 Computed Droplet Fallout for the 45.19 micron Droplet, U=175 mph.

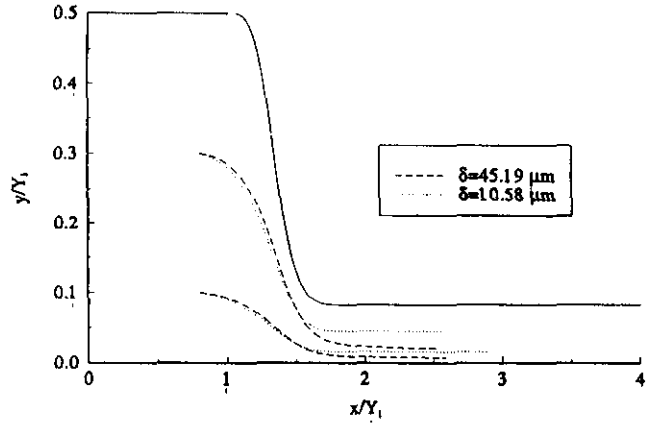

Fig. 10 Comparison of the Computed Trajectories for the 10.58 and 45.19 micron Droplets, U=175 mph.

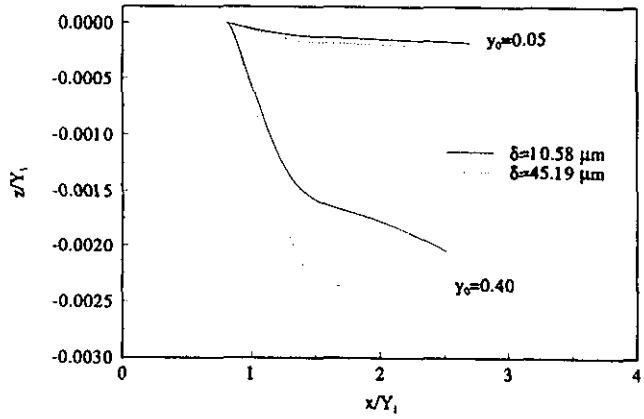

Fig. 13 Comparison of the Computed Fallout for the 10.58 and 45.19 micron Droplets, U=175 mph.

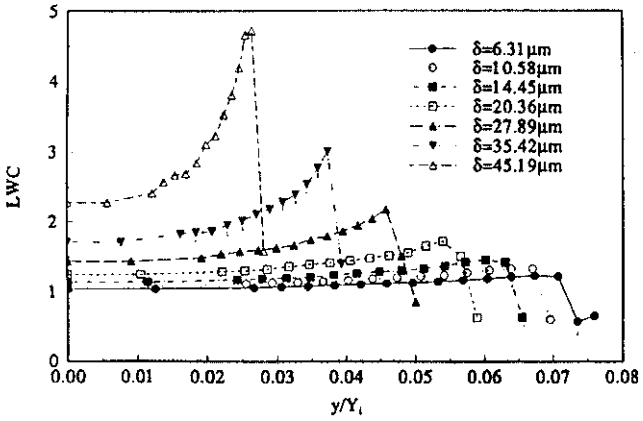

Fig. 14 Computed LWC's for the Droplets Across the Tunnel Test Section.

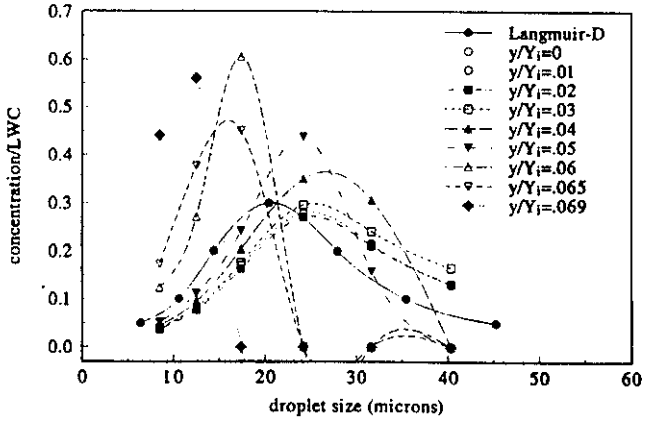

Fig. 17 Water Concentration Made Non-Dimensional with respect to the Langmuir-D Distribution.

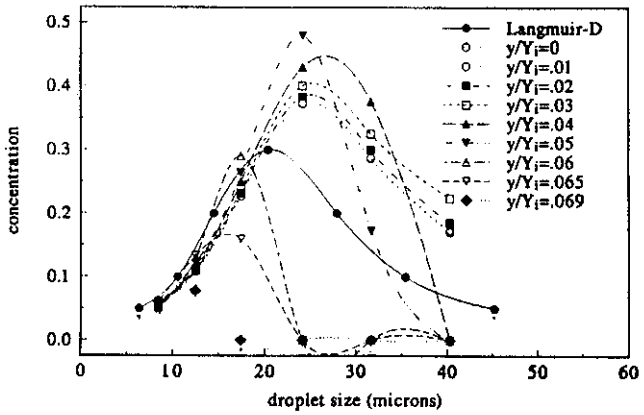

Fig. 15. Variation of Water Concentration as a Function of Droplet Size Distribution.

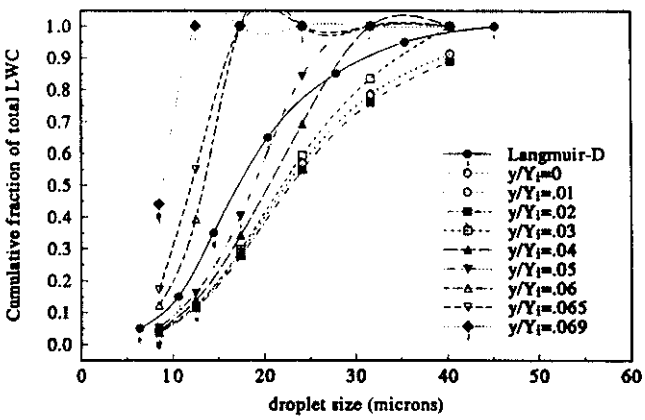

Fig. 18 Cumulative Fraction of Total LWC.

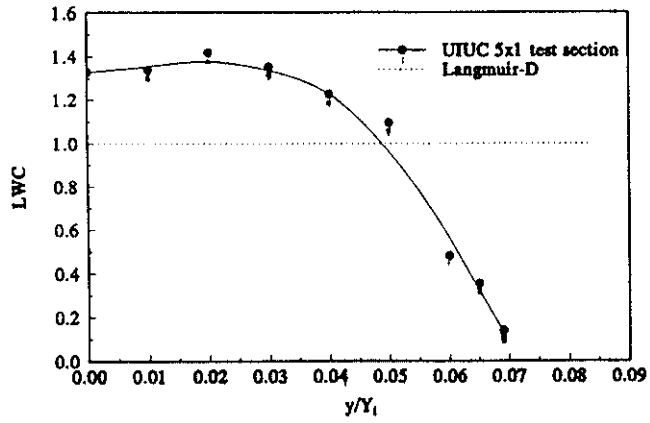

Fig. 16 Variation of LWC Across the Test Section.

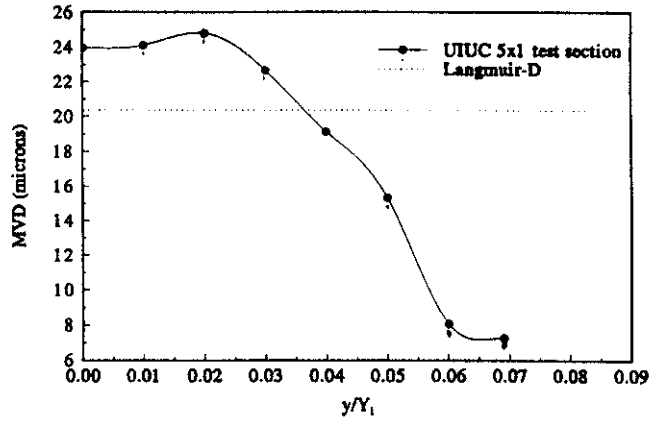

Fig. 19 Variation of Effective MVD Across the Test Section.